THE JOURNAL OF PHYSICAL CHEMISTRY C

Article

pubs.acs.org/JPCC

Cu-Doped ZnO Hemispherical Shell Structures: Synthesis and Room-Temperature Ferromagnetism Properties

D. H. Xu and W. Z. Shen*

Laboratory of Condensed Matter Spectroscopy and Opto-Electronic Physics, and Key Laboratory of Artificial Structures and Quantum Control (Ministry of Education), Department of Physics, Shanghai Jiao Tong University, 800 Dong Chuan Road, Shanghai 200240, China

ABSTRACT: We report a simple chemical vapor deposition method to fabricate Cu-doped ZnO hemispherical shell structures with room-temperature ferromagnetism (RTFM). Through a series of controlled experiments by changing the growth temperature and reaction time, we observe the evolution of product morphology from whole spherical structures into partially broken shells and hemispherical shells at different temperatures together with the reinforced hemispherical shells with the reaction time extended. The growth mechanism of the ZnO:Cu hemispherical shell structures has been proposed to involve the synthesis of Cu-doped Zn sphere, surface oxidation, and sublimation of the inner Zn from the broken shell. The structural and optical properties of the ZnO:Cu system with different Cu contents (below 4%) were investigated by X-ray diffraction, Raman spectroscopy, and photoluminescence measurements indicating that the Cu ions were successfully substituted into the Zn^{2+} lattice sites, and more intrinsic structural defects were introduced with the increase of the Cu content. X-ray photoelectron spectroscopy shows that the Cu ions are majorly in the cuprous state, which cannot contribute to ferromagnetism. We have attributed the origin of the enhanced RTFM with Cu contents in our ZnO:Cu hemispherical shell structures to the increased intrinsic lattice defects triggered by the Cu doping.

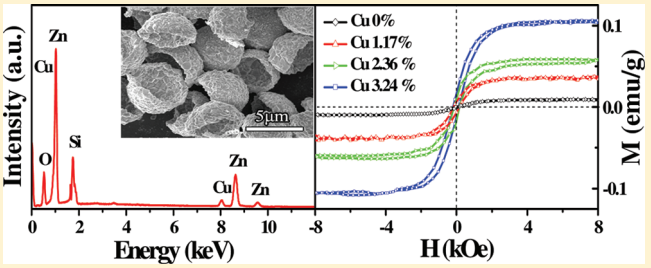

I. INTRODUCTION

Transition metal (TM) doped ZnO has recently attracted considerable attention for the potential application in spintronic devices because its Curie temperature is theoretically predicted to be well above room temperature[1,2] and room-temperature ferromagnetism (RTFM) has been observed experimentally in Co-,[3] Fe-,[4] Mn-,[5,6] and Cu-doped[7] ZnO systems. Among these TM doped magnetic semiconductors, Cu-doped ZnO (ZnO:Cu) is free of ferromagnetic impurities because neither metallic Cu nor its oxides are ferromagnetic leading to form an intrinsic dilute magnetic semiconductor.[8] In addition, the substitution of Zn by Cu in ZnO:Cu is a p-type doping,[9] which may promote RTFM, and the size mismatch between Cu and Zn is very small (~5%) resulting in the low formation energy.[10]

ZnO:Cu system with RTFM has been successfully realized through methods such as rf magnetron sputtering,[11] pulsed laser deposition,[7,12,13] ion beam technique,[14] filtered cathodic vacuum arc technique,[15] sol−gel method,[16] and chemical vapor deposition.[17−19] However, it remains controversial whether the observed ferromagnetism originates from the extrinsic Cu doping or the intrinsic structural defects of ZnO. Herng et al.[15] have shown that the origin of the ferromagnetism in Cu-doped ZnO films is mainly due to the Cu ions substituted into the ZnO lattice inducing the p−d hybridization between 3d of Cu and ZnO valence bands [O−p bands]. In contrast, Xu et al.[13] have observed that the ferromagnetism appears only in pure ZnO films (not in intentionally ZnO:Cu) and have concluded that the intrinsic defects, such as oxygen vacancies and defects of Zn sites, are responsible for the RTFM rather than the Cu dopant.

Most of the investigations of RTFM ZnO:Cu system have been focused on bulk materials or thin films, whereas only a few reports on nanostructures (e.g., nanoparticles,[20] nanowires,[17,18] nanonails, and nanoneedles[19]) have been published to date. These nanostructures have been known to have a longer spin lifetime than that of the film implying that they have great potential in nanoscale spintronic devices.[21] Compared with other one dimension ZnO nanostructures (nanowires, nanorods, nanonails, etc.), the hollow spherical structures have wide applications in many fields such as catalysis, sensors, drug delivery, energy-storage media, chemical/biological separation, sensing, and so forth because of their geometrically hollow shape and large surface area.[22] Nevertheless, there is no report on the Cu-doped hollow micro- and nanospherical structures with RTFM. It is difficult to prepare the hollow spherical ZnO structure with no aid of spherical template because of its different growth rates of ZnO crystal in different directions.

In this paper, we report on the successful synthesis of ZnO:Cu hollow spherical structures through a simple chemical vapor deposition method[6] at low temperatures of 580−650 °C. Detailed structural and optical studies reveal that Cu ions are

Received: January 12, 2012
Revised: April 7, 2012

   dx.doi.org/10.1021/jp3003849 | J. Phys. Chem. C XXXX, XXX, XXX−XXX

indeed substituted into the ZnO lattice existing mainly in univalent, which cannot produce p−d hybridization.[23] Because RTFM can be observed in both ZnO:Cu spherical structures and undoped one, we have attributed the origin of RTFM in our ZnO:Cu system to the increased intrinsic defects introduced by Cu doping.

II. EXPERIMENTAL DETAILS

ZnO:Cu hollow spherical structures were prepared on Si substrate by a simple chemical vapor deposition method in a horizontal tube furnace (150 cm long). Zn (99.99% purity) and $CuCl_2{\cdot}2H_2O$ (99.99% purity) powders were first mixed at an appropriate proportion as the source materials. The mixture was loaded into an alumina boat and was placed at the bottom of a one-end-sealed quartz tube (2 cm diameter, 70 cm long). Carefully cleaned n-type Si(100) substrates were then placed about 45 cm away from the source materials to receive the products. After that, the quartz tube was evacuated to ∼10 Pa using a mechanical rotary pump to remove the residual oxygen before heating. The heated temperature of the furnace was raised to 650 °C at a rate of 10 °C/min. When it reached the desired temperature, the carrying gas mixed with Ar (flow rate of 260 sccm) and O_2 (flow rate of 60 sccm) was introduced from the open end of the quartz tube. The duration of growth lasted for 30, 60, and 120 min. We finally obtained the deep yellow layer on the Si substrate after the quartz tube was cooled to room temperature naturally. For comparative studies, we also prepared the ZnO:Cu samples at heated temperatures of 580 and 620 °C as well as the undoped ZnO hollow spherical structure synthesized without copper source.

The morphology and structure of the ZnO:Cu hollow spherical structures were characterized using a field emission scanning electron microscope (FE-SEM; Philips XL30FEG) with an accelerating voltage of 5 kV, a high-resolution transmission electron microscope (HRTEM) (JEOL JEM-2100F), and X-ray diffraction (XRD) (Bruker/D8 Discover diffractometer with GADDS) with a Cu Kα source (λ = 1.5406 Å). Energy-dispersive X-ray (EDX) analysis was also performed during the FE-SEM observation. The bonding characteristics were analyzed by a PHI Quantum 2000 X-ray photoelectron spectroscopy (XPS). The micro-Raman in the backscattering geometry and the photoluminescence (PL) spectra were recorded at room temperature by a Jobin Yvon LabRAM HR800UV micro-Raman system under an Ar^+ (514.5 nm) and a He−Cd (325.0 nm) laser excitation, respectively. The measurements of the magnetic properties were carried out using a physical property measurement system (PPMS-12).

III. RESULTS AND DISCUSSION

We start from the Cu-doped ZnO hollow spherical structures synthesized by evaporating the mixture of Zn and $CuCl_2{\cdot}2H_2O$ powders at 650 °C for 120 min. The EDX analysis shown in Figure 1a indicates that the as-fabricated sample consists of Cu, Zn, and O with the Cu content 1.17%. The signal of Si originates from the substrate. Figure 1a′ presents the typical FE-SEM image of the as-prepared ZnO:Cu sample. We can observe that the sample obtained at 650 °C exhibits hemispherical shell structures with a uniform diameter of ∼5 μm. Moreover, it is found that the structures are accumulated by nanoparticles in the size of several hundred nanometers. To exploit the influence of the Cu dopant on the morphology of the synthesized products, we have also prepared the undoped

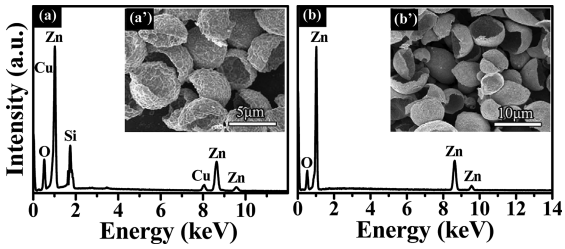

Figure 1. (a) EDX spectrum and (a′) FE-SEM image of hollow spherical structures with Cu (1.17%) doped ZnO; (b) EDX spectrum and (b′) FE-SEM image of undoped ZnO hollow spherical structures. The EDX spectrum in b was obtained from the powder scrapped off the silicon substrate unlike the doped case in a.

counterpart under the same experimental conditions with the exception of the Cu source. Figure 1b displays the EDX spectrum of the undoped ZnO sample demonstrating that the obtained structures are composed of only Zn and O elements. The corresponding typical morphology shown in Figure 1b′ also exhibits hemispherical shell shape with a relatively smooth surface. The diameter of the spherical shell is in the range of 5−8 μm with most distributed around 8 μm. Comparing Figure 1a′ with Figure 1b′, it is obvious that the hollow spherical structures get rougher on the surface and much more uniform in size after Cu doping.

To clarify the growth mechanism of the ZnO:Cu hemispherical shell structures, we have prepared different samples by adjusting the temperature of the source materials and the reaction time. As seen from the SEM images in Figure 2a−c, three different kinds of ZnO:Cu spherical structures were realized after the reaction was carried out at 580, 620, and 650 °C for 120 min, respectively. At the temperature of 580 °C (Figure 2a), the as-synthesized sample exhibits sealed microspheres with a diameter of about 1 μm. When the reaction temperature increases to 620 °C, the as-prepared ZnO:Cu microspheres shown in Figure 2b are partly opened with a shell thickness of about 1 μm and a uniform size of ∼2 μm. Further increasing the temperature to 650 °C (Figure 2c), the diameter of the hollow microsphere becomes larger (5 μm) and the opened shell of the hollow sphere is thinner (600 nm) than that of the microspheres at 620 °C. It is clear that with the increase of reaction temperature, the products are changed from sealed microspheres at 580 °C to partially opened spherical structures at 620 °C and to hemispherical shells at 650 °C together with the corresponding spherical microstructures becoming larger in size and thinner in the thickness of the shell.

We have also prepared the ZnO:Cu samples by changing the reaction time from 30 to 120 min at 650 °C to observe the morphology evolution with the reaction time. Loose Cu-doped ZnO hemispherical structures with lots of holes were obtained at the reaction time of 30 min (Figure 2d) indicating that at an early stage a sparse layer of Cu-doped ZnO nanoparticles was synthesized. Relatively reinforced hemispherical shells can be observed in Figure 2e for the sample prepared for 60 min. Compared with the morphologies of the samples produced for 120 min in Figure 2c, the structures of the products were found to be reinforced with the extension of reaction time.

Transmission electron microscopy (TEM) observation is helpful to further understand the crystalline structures of the hollow spherical structures. Figure 2f shows the typical TEM image of a single hollow hemisphere shell structure produced at 650 °C for 120 min with the Cu content 1.17%, which clearly

dx.doi.org/10.1021/jp3003849 | J. Phys. Chem. C XXXX, XXX, XXX−XXX

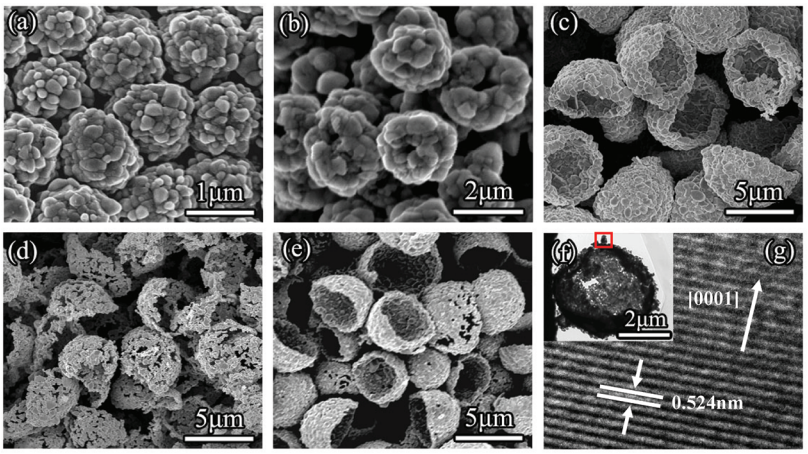

Figure 2. (a–c) FE-SEM images of hollow spherical ZnO:Cu structures prepared at 580, 620, and 650 °C for 120 min, respectively; (d, e) FE-SEM images of hollow spherical ZnO:Cu structures prepared at 650 °C for 30 and 60 min, respectively; (f) TEM image and (g) HRTEM of Cu (1.17%) doped ZnO hollow spherical structures.

reveals that the microspheres are hollow and have a relatively smooth surface. Figure 2g is the lattice-resolved HRTEM image of the selected Cu-doped nanoparticle indicated in Figure 2f with a red rectangle. The lattice fringe is about 0.524 nm, which corresponds to the [0001] crystal planes of wurtzite ZnO. It indicates that the ZnO:Cu nanoparticle is single crystalline and that the growth direction is perpendicular to the [0001] plane.

From the above observation and the previously reported results on the synthesis of pure ZnO hollow microspheres,[24,25] we suggest the following possible growth mechanism of the ZnO:Cu hollow spherical structures. Cu-doped Zn spheres were first synthesized through the Zn and Cu vapor depositing on Si substrates. When the oxygen is introduced into the quartz tube at a desired temperature, the outside layer of the Cu-doped Zn spheres was quickly oxidized forming a sparse layer of ZnO:Cu nanoparticles. Because the temperature of the substrate was higher than the melting point of Zn (419 °C), inner Zn could be further sublimed from the holes of the sparse layer and was simultaneously oxidized to form a dense ZnO:Cu layer leading to the formation of hollow spherical structures. This argument can also be confirmed in Figure 2c–e that with the time extended, the structures became more and more compact. As we know, as the inner pressure generated by the Zn steam increases with the reaction temperature (from 580 to 650 °C), the weakest part of the outside ZnO:Cu layer is apt to break up to balance the pressure in and out. As a result, the whole spherical structures (Figure 2a) grew into partially broken shells (Figure 2b) and hemispherical shells (Figure 2c) with the increasing pressure difference.

We have successfully realized the synthesis of Cu-doped ZnO hemispherical shell structures with different Cu contents (below 4%, including undoped ZnO one). Figure 3a presents the typical XRD pattern of the yielded ZnO:Cu hemispherical shell structures. It is clear that all the diffraction peaks can be indexed to the hexagonal wurtzite structure of ZnO (JCPD No. 36-1451) coincident with the above HRTEM observation. No other peaks corresponding to copper and its related secondary or impurity phase were found in the ZnO:Cu samples revealing that the substitution of copper does not affect the wurtzite structure of zinc oxide.[26] Typically, with the increase of Cu content, the XRD peaks of Cu-doped samples have constantly shifted slightly toward lower scattering angle indicating an increase of the lattice constant which can be attributed to the

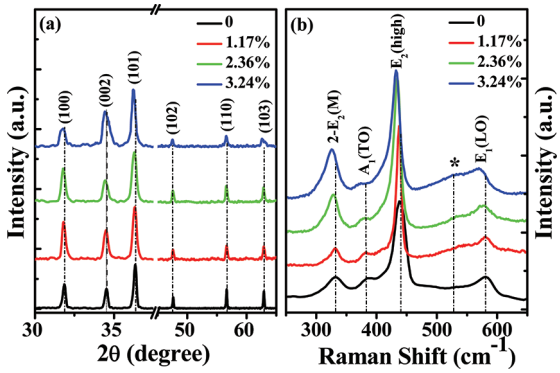

Figure 3. (a) XRD and (b) Raman spectra of undoped ZnO and Cu-doped hemispherical shell structures with Cu contents of 1.17, 2.36, and 3.24%.

nonuniform substitution of Cu ion into the Zn site as the radius of Cu ion (0.057 nm) is smaller than that of the Zn ion (0.06 nm).[27] The unusual shift results from the lattice distortion caused by the stress during the preparation.[28] A similar observation has been found in Cu-doped ZnO nanowire arrays[29] and Co-doped ZnO bulk materials.[30]

Figure 3b shows the Raman spectra of the as-prepared samples with different Cu contents in the range 250–650 cm^{-1} measured at room temperature. In the undoped ZnO sample, the peak at about 330 cm^{-1} can be assigned to the second-order acoustic mode [2-E_2(M)], that at 384 cm^{-1} to A_1 transverse optical (TO) mode [A_1(TO)], and that at ~580 cm^{-1} to E_1 longitudinal optical (LO) mode [E_1(LO)]. The sharp and high peak around 437 cm^{-1} corresponds to the nonpolar optical phonon E_2(high) mode of ZnO, which is related to the motion of oxygen atoms and is a typical Raman active branch of wurtzite ZnO.[31] The presence of the E_2(high) mode in all the four samples indicates the hexagonal wurtzite structure, which is consistent with the above HRTEM and XRD analysis. It can be seen that the E_1(LO) mode of Cu-doped ZnO samples shifts to lower frequency after doping resulting from the destruction of the long-range order in ZnO by the Cu dopant. In comparison with the Raman spectrum of pure ZnO, an additional mode that is indicated as "*" at around 530–540 cm^{-1} is observed in the Cu-doped ZnO samples, which can be attributed to the lattice defects triggered by the incorporation of

dx.doi.org/10.1021/jp3003849 | J. Phys. Chem. C XXXX, XXX, XXX–XXX

Cu ions into the ZnO.[32] Moreover, the intensity of the additional peak increases with the Cu content suggesting that more and more lattice defects are introduced by the Cu doping.

We now turn to investigate the magnetic properties of the undoped and Cu-doped ZnO hemispherical shell structures. Figure 4 shows the magnetization versus magnetic field (M−H)

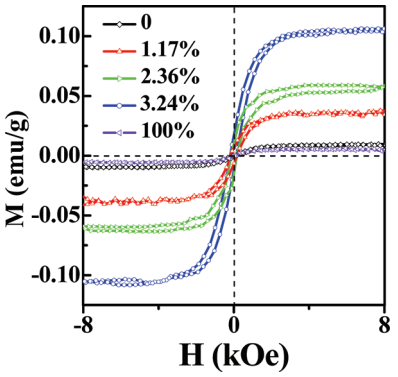

Figure 4. M−H curves at 300 K of undoped ZnO and Cu-doped hemispherical shell structures with Cu contents of 1.17, 2.36, 3.24, and 100% (pure copper oxide).

loops at room temperature (300 K) in the field range of 0 ∼ ±8kOe for the different Cu contents of the yielded samples. It is clear that RTFM can be observed in not only all the three different Cu contents of ZnO:Cu samples but also the undoped ZnO one. There are some reports in the literature on RTFM in pure ZnO films,[33] nanoparticles,[34] and nanowires,[35] where the observed ferromagnetism has been attributed to the local magnetic moment of intrinsic defects, such as the Zn interstitials and O vacancies. However, RTFM in undoped ZnO hemispherical shell structures has not been reported before. From an application point of view, the synthesis of ferromagnetism hemispherical shell structures is very important because of their unique hollow structures. In addition, the M−H characteristics in Figure 4 demonstrate that the saturation magnetization of the ZnO:Cu semispherical shell structures increases noticeably with the Cu content of the samples. In other words, the saturation magnetization in ZnO:Cu semispherical shell system can be tuned by controlling the Cu content.

For further comparative study of the effect of copper, we have also prepared the pure copper oxide nanostructures in the same condition as ZnO:Cu hemispherical shell structures without Zn source. They have exhibited very weak ferromagnetism (∼0.006 emu/g) at 300 K (noted as 100% Cu content in Figure 4). For comparison, the corresponding saturated magnetizations are 0.036, 0.058, and 0.105 emu/g for the as-prepared ZnO:Cu hemispherical shell structures with low Cu concentrations of 1.17, 2.36, and 3.24%, respectively. Furthermore, there are no observable Cu-related secondary phases existing in the ZnO:Cu structures, which have been confirmed by the results of TEM (Figure 2), XRD, and Raman (Figure 3) spectroscopy. On the basis of the above results, we can draw the conclusion that the influence of the Cu-based secondary phases can be neglected for the observed RTFM. On the other hand, the structural XRD and Raman characterization in Figure 3 have provided unambiguous evidence of the substitution of Cu in Zn lattice site and of more and more lattice defects introduced with the increase of Cu content in the as-prepared ZnO:Cu system. In combination with the magnetism characteristics in Figure 4 and the structural properties in Figure 3, a question is raised whether the observed ferromagnetism is due to the substitution of Cu or to the defects introduced by the Cu doping. To clarify the origin of the ferromagnetism in ZnO:Cu hemispherical shell structures, we resort to the XPS measurements to examine the valence state of copper and to the PL spectra to study the defect properties after the Cu doping.

Figure 5 presents the high-resolution XPS spectrum of the synthesized ZnO:Cu hemispherical shell structures with the

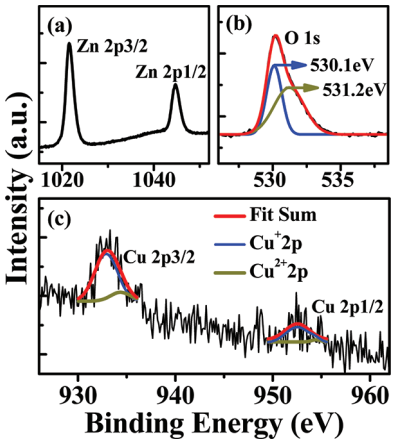

Figure 5. High-resolution XPS spectra of (a) Zn 2p, (b) O 1s, and (c) Cu 2p in hemispherical shell structures of Cu (3.24%) doped ZnO.

highest Cu content of 3.24%. As shown in Figure 5a, the XPS spectrum of Zn 2p reveals the binding energies of Zn 2p3/2 at about 1021.5 eV and Zn 2p1/2 centered at 1044.7 eV without any noticeable shift after the Cu doping.[36] The XPS spectrum of O 1s (Figure 5b) is asymmetric indicating the presence of multicomponent oxygen species. We can fit the XPS structure with two components, which are centered at 530.1 and 531.2 eV, respectively. The former is attributed to the oxygen ions in the crystal lattice while the latter is associated with adsorbed oxygen.[37] Figure 5c shows the Cu 2p XPS spectrum of the synthesized ZnO:Cu hemispherical shell structures. Cu 2p3/2 and Cu 2p1/2 of the sample are found to locate at 933.1 and 952.5 eV, respectively, similar to the results of Cu-doped ZnO nanowires.[14] The dominated peaks can be Gaussian fitted with major cuprous Cu^+ (fixing 2p3/2 peak at 932.9 eV and 2p1/2 peak at 952.5 eV) and extremely minor Cu^{2+} (fixing 2p3/2 peak at 934.3 eV and 2p1/2 peak at 954.5 eV) components, which is consistent with the result reported by Shuai et al.[38] As we know, all electrons are paired in the $3d^{10}$ configuration of Cu^+ ion, and hence, Cu^+ cannot produce a magnetic moment.[23] Therefore, the origin of the RTFM in our ZnO:Cu system cannot be due to the major cuprous Cu^+ substitution.

We finally find out the answer by the aid of the room-temperature PL measurements on these undoped and Cu-doped ZnO semispherical shell structures with different Cu contents through exploring the role played by the defects in tuning the magnetic properties. As shown in Figure 6, all the samples show two distinct emission peaks: a sharp one in the ultraviolet (UV) region and another broad one in the visible region. The former is attributed to exciton-related near-band-edge luminescence while the latter is generally referred to deep-level emission.[39] For the pure ZnO sample, the visible luminescence is generally referred to the recombination of a

dx.doi.org/10.1021/jp3003849 | J. Phys. Chem. C XXXX, XXX, XXX−XXX

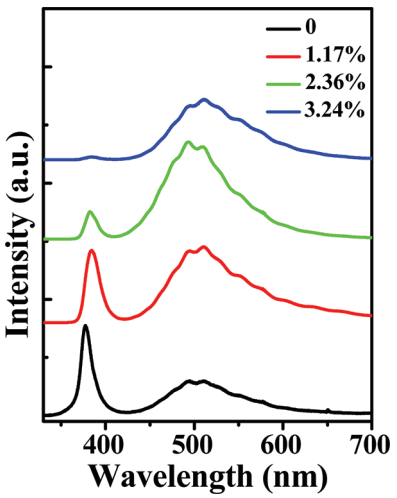

Figure 6. Room-temperature PL spectra of undoped ZnO and Cu-doped hemispherical shell structures with Cu contents of 1.17, 2.36, and 3.24%.

photogenerated hole with the singly ionized oxygen vacancy, and its intensity could be used as an indicator of the oxygen vacancy concentration in ZnO.[40] We can observe that the undoped ZnO possesses a strong near band edge UV emission together with a weak visible emission indicating that the synthesized undoped ZnO hemispherical shell structures have a fairly high quality with low oxygen vacancy concentration. The presence of Cu rapidly reduces the UV emission of ZnO:Cu samples and broadens the peak toward longer wavelengths compared with the undoped counterpart. The UV peaks of undoped and doped ZnO hemispherical shell structures are located at 377 and 384 nm, respectively. The redshift of ~7 nm in the Cu-doped samples, that is, a reduction of ZnO band gap caused by the Cu doping, also indicates the substitution of Cu ions on Zn sites in the lattice. Similar results have been reported by He et al.[41] in Ni-doped ZnO nanowires. Notably, the UV peaks in doped samples are suppressed severely because of Cu doping while the visible luminescence is enhanced by Cu ions because of the poorer crystallinity and greater level of structural defects, which were attributed to more intrinsic defects introduced by Cu ion incorporation into ZnO. The intensity ratio of the visible band emission to the UV peak enhances from ~0.38 to ~20 with the Cu content change from 0 to 3.24% demonstrating that the Cu doping strongly increases the concentration of defects. This result is consistent with the above Raman observation that the lattice defects are generated gradually with the Cu doping.

With the above PL observation and the structural properties in Figures 3 and 5, we go back to the magnetic properties of the as-prepared samples in Figure 4, which demonstrates that the undoped ZnO sample shows very weak magnetic properties and that the saturation magnetization of the ZnO:Cu semispherical shell structures increases gradually with the Cu content. The observation of RTFM in the undoped ZnO sample indicates that the ferromagnetism originates from the local magnetic moment of intrinsic structural defects. The presence of low concentration (below 4%) Cu in ZnO does not favor the conventional superexchange or double-exchange interactions to produce long-range magnetic order.[42] From the Cu ionic valence state by XPS, we have found that the Cu ions are mainly in the cuprous state, which cannot induce the p−d hybridization between 3d of Cu and ZnO valence bands [O−p bands]. Hence, the substitution of Zn^{2+} by cuprous Cu^{+} does not likely contribute directly to ferromagnetism, but it introduces more intrinsic structural defects, which has been confirmed by our Raman and PL data in these ZnO:Cu samples. The defect concentration could play very important roles in enhancing the magnetism,[43,44] which has been observed in Cu-doped ZnO films,[13] nanonails, and nanoneedles.[19] Gao et al.[45] have also reported that the $Zn_{0.93}Cu_{0.07}O$ nanowires annealed in vacuum have much stronger ferromagnetism than that annealed in air indicating that more oxygen vacancy defects are responsible for the enhancement of ferromagnetism. Therefore, we attribute the origin of RTFM in our ZnO:Cu samples to intrinsic defects because the concentrations of defects are significantly increased with the Cu doping in the as-prepared ZnO:Cu system.

IV. CONCLUSION

In summary, we have developed a simple chemical vapor deposition method to synthesize Cu-doped ZnO hemispherical shell structures with RTFM. The morphology of the products grew into sealed microspheres or partially opened spherical structures at different temperatures and was found to be reinforced with the reaction time extended. The hollow spherical structures became rougher on the surface and much more uniform in size after Cu doping. The growth mechanism has been proposed to involve the synthesis of Cu-doped Zn sphere, surface oxidation, and sublimation of the inner Zn from the broken shell. We have employed TEM, XRD, and Raman spectroscopy to demonstrate that the hemispherical structures are composed of single crystalline ZnO:Cu nanoparticles and to confirm that the Cu ions successfully substituted in Zn^{2+} lattice sites while maintaining the wurtzite structure. Both the undoped and Cu-doped ZnO semispherical shell structures exhibit RTFM, and the ferromagnetism increases gradually with the Cu content. However, the XPS results show that the Cu ions are mainly in the cuprous state, which cannot contribute to ferromagnetism for its fully occupied d shell. Furthermore, the additional mode in Raman spectra at around 530−540 cm^{-1} is related to the visible emission in their PL spectra, which is generated from intrinsic defects created by the Cu incorporation into ZnO. As a result, we have attributed the origin of the observed RTFM in our ZnO:Cu hemispherical shell structures to more lattice defects introduced with the increase of Cu content. The present method is expected to be employed in a broad range to fabricate other TM doped ZnO hemispherical shell structures for potential application in spintronic devices.

AUTHOR INFORMATION

Corresponding Author

*E-mail: wzshen@sjtu.edu.cn.

Notes

The authors declare no competing financial interest.

ACKNOWLEDGMENTS

This work was supported by the National Major Basic Research Project of 2012CB934302 and the Natural Science Foundation of China under contracts 11074169 and 11174202.

REFERENCES

(1) Dietl, T.; Ohno, H.; Matsukura, F.; Cibert, J.; Ferrand, D. *Science* **2000**, *287*, 1019.

(2) Sato, K.; Katayama-Yoshida, H. *Semicond. Sci. Technol.* **2002**, *17*, 367.
(3) Lee, H. J.; Jeong, S. Y. *Appl. Phys. Lett.* **2002**, *81*, 4020.
(4) Karmakar, D.; Mandal, S. K.; Kadam, R. M.; Paulose, P. L.; Rajarajan, A. K.; Nath, T. K.; Das, A. K.; Dasgupta, I.; Das, G. P. *Phys. Rev. B* **2007**, *75*, 144404.
(5) Sharma, P.; Gupta, A.; Rao, K. V.; Owens, F. J.; Sharma, R.; Ahuja, R.; Guillen, J. M.; Johansson, B.; Gehring, G. A. *Nat. Mater.* **2003**, *2*, 673.
(6) Lin, X. X.; Zhu, Y. F.; Shen, W. Z. *J. Phys. Chem. C* **2009**, *113*, 1812.
(7) Buchholz, D. B.; Chang, R. P. H.; Song, J. H.; Ketterson, J. B. *Appl. Phys. Lett.* **2005**, *87*, 082504.
(8) Wei, M.; Braddon, N.; Zhi, D.; Midgley, P. A.; Chen, S. K.; Blamire, M. G.; MacManus-Driscoll, J. L. *Appl. Phys. Lett.* **2005**, *86*, 072514.
(9) Ye, L. H.; Freeman, A. J.; Delley, B. *Phys. Rev. B* **2006**, *73*, 033203.
(10) Ahn, K. S.; Deutsch, T.; Yan, Y.; Jiang, C. S.; Perkins, C. L.; Turner, J.; Al-Jassim, M. *J. Appl. Phys.* **2007**, *102*, 023517.
(11) Hou, D. L.; Ye, X. J.; Zhao, X. Y.; Meng, H. J.; Zhou, H. J.; Li, X. L.; Zhen, C. M. *J. Appl. Phys.* **2007**, *102*, 033905.
(12) Li, X. L.; Xu, X. H.; Quan, Z. Y.; Guo, J. F.; Wu, H. S.; Gehring, G. A. *J. Appl. Phys.* **2009**, *105*, 103914.
(13) Xu, Q.; Schmidt, H.; Zhou, S.; Potzger, K.; Helm, M.; Hochmuth, H.; Lorenz, M.; Setzer, A.; Esquinazi, P.; Meinecke, C.; Grundmann, M. *Appl. Phys. Lett.* **2008**, *92*, 082508.
(14) Herng, T. S.; Lau, S. P.; Yu, S. F.; Yang, H. Y.; Wang, L.; Tanemura, M.; Chen, J. S. *Appl. Phys. Lett.* **2007**, *90*, 032509.
(15) Herng, T. S.; Lau, S. P.; Yu, S. F.; Yang, H. Y.; Ji, X. H.; Chen, J. S.; Yasui, N.; Inaba, H. *J. Appl. Phys.* **2006**, *99*, 086101.
(16) Lee, H. J.; Kim, B. S.; Cho, C. R.; Jeong, S. Y. *Phys. Status Solidi B* **2004**, *241*, 1533.
(17) Xu, C.; Yang, K.; Huang, L.; Wang, H. *J. Chem. Phys.* **2009**, *130*, 124711.
(18) Xing, G. Z.; Yi, J. B.; Tao, J. G.; Liu, T.; Wong, L. M.; Zhang, Z.; Li, G. P.; Wang, S. J.; Ding, J.; Sum, T. C.; Huan, C. H. A.; Wu, T. *Adv. Mater.* **2008**, *20*, 3521.
(19) Zhang, Z.; Yi, J. B.; Ding, J.; Wong, L. M.; Seng, H. L.; Wang, S. J.; Tao, J. G.; Li, G. P.; Xing, G. Z.; Sum, T. C.; Huan, C. H. A.; Wu, T. *J. Phys. Chem. C* **2008**, *112*, 9579.
(20) Liu, H. L.; Yang, J. H.; Zhang, Y. J.; Wang, Y. X.; Wei, M. B.; Wang, D. D.; Zhao, L. Y.; Lang, J. H.; Gao, M. *J. Mater. Sci.: Mater. Electron.* **2009**, *20*, 628.
(21) Kane, M. H.; Strassburg, M.; Asghar, A.; Song, Q.; Gupta, S.; Senawiratne, J.; Hums, C.; Haboeck, U.; Hoffmann, A.; Azamat, D.; Gehlhoff, W.; Dietz, N.; Zhang, Z. J.; Summers, C. J.; Ferguson, I. T. *Proc. SPIE* **2005**, *5732*, 389.
(22) Zhu, Y. F.; Fan, D. H.; Shen, W. Z. *J. Phys. Chem. C* **2007**, *111*, 18629.
(23) Chakraborti, D.; Narayan, J.; Prater, J. T. *Appl. Phys. Lett.* **2007**, *90*, 062504.
(24) Sulieman, K. M.; Huang, X. T.; Liu, J. P.; Tang, M. *Nanotechnology* **2006**, *17*, 4950.
(25) Gao, P. X.; Wang, Z. L. *J. Am. Chem. Soc.* **2003**, *125*, 11299.
(26) Xu, C. X.; Sun, X. W.; Zhang, X. H.; Ke, L.; Chua, S. J. *Nanotechnology* **2004**, *15*, 856.
(27) Shannon, R. D. *Acta Crystallogr.* **1976**, *A32*, 751.
(28) Ozen, I.; Gulgun, M. A. *Adv. Sci. Technol.* **2006**, *45*, 1316.
(29) Gao, D. Q.; Xue, D. S.; Xu, Y.; Yan, Z. J.; Zhang, Z. H. *Electrochim. Acta* **2009**, *54*, 2392.
(30) Kolesnik, S.; Dabrowski, B.; Mais, J. *J. Appl. Phys.* **2004**, *95*, 2582.
(31) Cao, B. Q.; Cai, W. P.; Zeng, H. B.; Duan, G. T. *J. Appl. Phys.* **2006**, *99*, 073516.
(32) Phan, T. L.; Vincent, R.; Cherns, D.; Nghia, N. X.; Ursaki, V. V. *Nanotechnology* **2008**, *19*, 475702.
(33) Hong, N. H.; Sakai, J.; Brizé, V. *J. Phys: Condens. Matter* **2007**, *19*, 036219.
(34) Gao, D. Q.; Zhang, Z. H.; Fu, J. L.; Xu, Y.; Qi, J.; Xue, D. *J. Appl. Phys.* **2009**, *105*, 113928.
(35) Xing, G. Z.; Wang, D. D.; Yi, J. B.; Yang, L. L.; Gao, M.; He, M.; Yang, J. H.; Ding, J.; Sum, T. C.; Wu, T. *Appl. Phys. Lett.* **2010**, *96*, 112511.
(36) Xu, H. Y.; Liu, Y. C.; Xu, C. S.; Liu, Y. X.; Shao, C. L.; Mu, R. *Appl. Phys. Lett.* **2006**, *88*, 242502.
(37) Jin, Y. X.; Cui, Q. L.; Wen, G. H.; Wang, W. S.; Hao., J.; Wang, S.; Zhang, J. *J. Phys. D: Appl. Phys.* **2009**, *42*, 215007.
(38) Shuai, M.; Liao, L.; Lu, H. B.; Zhang, L.; Li, J. C.; Fu, D. J. *J. Phys. D: Appl. Phys.* **2008**, *41*, 135010.
(39) Huang, M. H.; Wu, Y. Y.; Feick, H.; Tran, N.; Weber, E.; Yang, P. D. *Adv. Mater.* **2001**, *13*, 113.
(40) Vanheusden, K.; Warren, W. L.; Seager, C. H.; Tallant, D. R.; Voigt, J. A.; Gnade, B. E. *J. Appl. Phys.* **1996**, *79*, 7983.
(41) He, J. H.; Lao, C. S.; Chen, L. J.; Davidovic, D.; Wang, Z. L. *J. Am. Chem. Soc.* **2005**, *127*, 16376.
(42) Coey, J. M. D.; Venkatesan, M.; Fitzgerald, C. B. *Nat. Mater.* **2005**, *4*, 173.
(43) Hong, N. H.; Sakai, J.; Huong, N. T.; Poirot, N.; Ruyter, A. *Phys. Rev. B* **2005**, *72*, 045336.
(44) Tian, Y. F.; Li, Y. F.; He, M.; Putra, I. A.; Peng, H. Y.; Yao, B.; Cheong, S. A.; Wu, T. *Appl. Phys. Lett.* **2011**, *98*, 162503.
(45) Gao, D. Q.; Xu, Y.; Zhang, Z. H.; Gao, H.; Xue, D. *J. Appl. Phys.* **2009**, *105*, 063903.